Critical Response To: Performance of Perovskite $CsPbBr_3$ Single Crystal Detector for Gamma-Ray Detection

1 INTRODUCTION

Early work of halide perovskites in solar cell research, where they have been proved to be an effective family of materials for increasing power conversion efficiency, gained the attention of research groups seeking new alternative radiation detectors since they possess outstanding optoelectronic properties. Specifically, metal halide perovskites were ideal candidates for direct (semiconductor) and indirect (scintillator) radiation detection for their high charge carrier mobility, long diffusion length, tunable bandgap, high quantum yield, high absorption coefficient, and flexible chemistry. Nonetheless, in the last couple of years, significant improvements have been made towards the field of ionized radiation detection through metal or non-metal halide perovskites. Through their processing versatility, a broad range of possible hybrid and inorganic perovskites were possible for researchers to discover and advance the field of high radiation detector technologies. These perovskites come in the form of nano-particles/wires/sheets, polycrystalline thin films, and bulk single crystals; the latter two being most popular in ionized radiation detection (e.g., alpha particle, X-ray, and gamma).

Perovskites consist of a large family of materials and are divided based on their chemical composition and structure; most notably in 3D and 2D form. These different structures represent the structural dimensionality of halide perovskites at the molecular level. The more traditional 3D halide perovskite has a general formula of ABX_3 where A can be a small organic cation (e.g., MA+ = methylammonium (CH3NH3 +), FA+ = formamidinium (CH $(NH_2)_2$ +)) or an inorganic cation (e.g., Cs+ , Rb+), B is a metal cation (e.g., Pb2+, Sn2+), and X is a halide anion (I−, Br−, Cl−). Thus, depending on whether the A cation is an inorganic or organic molecule determines perovskites' classification as inorganic or hybrid metal halide perovskites, respectively. In comparison to hybrid halide perovskites, inorganic perovskites have better thermal stability and lower ion migration thus are preferred for high energy radiation detection.[1] To predict the stability of the perovskite lattice, two factors are often used for perovskite formability and stability, see equation 1 and 2 respectively. The first is the tolerance (t) introduced by Goldschmit in 1926, where the ionic radii (r) of A is ($\mathrm{r_A}$), B is ($\mathrm{r_B}$), and X is ($\mathrm{r_X}$), and the seconde factor is known the octahedral factor (μ). The ranges of these two factors are provided where they are found to be empirically best to form and stabilize, respectively.

$$t = \frac{(\mathrm{r_A} + \mathrm{r_X})}{[\sqrt{2}\,(\mathrm{r_B} + \mathrm{r_X})]}, 0.81 \leq \mathrm{t} \leq 1.0 \quad (1),$$

$$\mu = \frac{\mathrm{r_B}}{\mathrm{r_A}}, 0.44 \leq \mu \leq 0.8 \quad (2). \text{ [1]}$$

Generally, 3D perovskites have shown little efficient scintillation at room temperature due to low exciton binding energy which causes thermal quenching, thus are best served for direct or semiconductor radiation detectors in bulk crystal form. In contrast, reducing the structural 3D to 2D perovskites leads to strong quantum confinement effects and deep excitonic levels that ensures efficient scintillation at room temperature, thus are best served for indirect scintillator radiation detectors.[2] It is the aim of this work to review the performance of an inorganic semiconductor $CsPbBr_3$ single crystal material for gamma ray detection based on digital pulse processing (DPP) by Lei et al. in 2020.[3] This halide perovskite materials has gained much attention due to its superior stability over its hybrid counterparts and thus been explored for wide range radiation detection. Before the report is presented, a brief theoretical section on gamma radiation detectors, recent advancements in solution growth of $CsPbBr_3$ single crystals for photo response, and properties of digital pulse processing are provided.

2 BACKGROUND

2.1. Gamma Radiation Detectors

Gamma radiation detection is vital for numerous applications such as medical imaging, homeland security, and astronomy. For these kind of applications, high resolution radiation detectors are necessary for precise identification and quantification of radioactive isotopes. There are two primary types of high energy radiation detectors which can be classified namely as direct or indirect detectors. Direct detection depends on the photoconductive materials that is sensitive to high energy radiation. Indirect detection employs scintillator materials that converted incoming energy radiation to ultraviolet (UV) or visible which then is detected by photodiodes. To understand the employment of these types of detectors for gamma ray detection, it's important to understand the fundamental gamma-ray interactions within a given medium. [1]

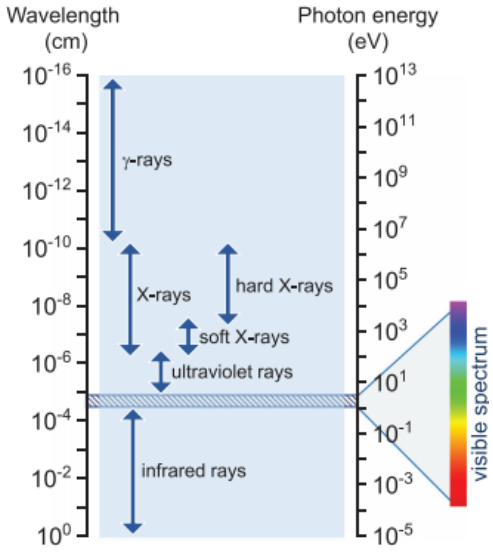

Figure 1. Electromagnetic spectrum between infrared and gamma rays along with their respective wavelengths and photon energies. [1]

Gamma ray radiation is comprised of high energy photons, see Figure 1, and have three main mechanisms to describe their interaction: photoelectric process, Compton Scattering, and pair production. The photoelectric effect describes the interaction in which the gamma ray fully deposits its kinetic energy E_γ into an atomic electron which leads to the ejection of liberated photoelectron (as well as generation of holes) that can be detected with kinetic energy $E_e = E_\gamma - E_b$ (where E_b is the electron's binding energy to the atomic nucleus). However, the binding energy is not lost and appears as a characteristic x-ray that also is absorbed within the detector. This type of interaction is most desirable for spectroscopic applications because it ensures fully energy deposition that is directly attributed to incident gamma photon. The gamma interaction probability in the material is directly proportional to Z^4 / E_γ^3 (E_γ is the gamma ray energy), hence compounds with high-Z elements are desirable for radiation detectors. Accordingly, photoelectric effect can be observed to dominate at low energies because of the inverse relationship with energy, between 10 and 500 keV. Compton scattering is the process where part of the gamma ray energy is lost and imparts some kinetic energy to a free or bound electron and in the process emitting a weakened gamma ray in a different trajectory. This process uses weakly bound electrons for scattering and is dominate for photons with energies between 50keV to 3 MeV. Pair production occurs when an incident gamma ray photon with energy 1.022 MeV or above interacts with an atomic nucleus generating an electron-positron pair which are then slowed down generating two 511 keV gamma rays to conserve momentum. For photon flux containing many photons, attenuation in the medium can be described by the following relationship,

$$I = I_0 e^{-\mu x} \quad (3)$$

where $I_0$is the original radiation intensity, μ is the absorption coefficient contributed by the abovementioned processes, and x is the absorption length of material. [4]

Now that the interactions are understood, the energy imparted to the photoelectron must be converted into a signal which can be interpreted to determine the energy of the incident gamma ray. Direct detectors which are comprised of semiconductors and electrodes that directly generate signals by the collection electron-hole pairs which then drift to their respective pole when an electric field is applied.[5] For detection of higher energy photons like that of gamma rays, certain characteristics are required of semiconductors:

1) Large stopping power to ensure ionization before escaping material: high Z elements (Z>40) and high density ($\rho > 5 \frac{g}{cm^3}$),
2) A preferable band gap to minimize intrinsic carriers from background (noise) and to generate more electron-hole pairs for the same incident energy according to the empirical formula of pair creation energy $\mathcal{E}_{pc} = 3E_g^{10}$ (1.5eV<E_g<3 eV),
3) High resistivity (>$10^9\ \Omega cm$) to permit high voltage bias to increase charge collection efficiency (CCE) and enhance the signal-to-noise ratio (smaller dark current),

4) Large carrier mobility-lifetime products $(\mu\tau)_e, (\mu\tau)_h$ ($\approx 10^{-2}\frac{cm^2}{V}$): in which mobility μ is inversely related to effective mass which in turn depend on electronic band structure (desirable widely dispersive bands at conduction band minimum and valence band maximum) that lead to low electron and hole effective masses, thus high charge carrier mobility. Charge carrier lifetime τ however is inversely proportional to defect concentration and thus if lowered would increase τ. [5]

Direct gamma ray or semiconductors detection utilizes spectroscopic techniques to be able to distinguish specific radiative isotopes from the photon emission. Voltage mode operation is used in this type of detector as the photon flux intensity is weak as the high energy photons come to the detector one by one. A preamplifier is employed due to the weak intensity of the signal to integrate the detector signal at given interval times. For pulse-height energy spectroscopy, a linear pulse shaping amplifier is employed to accept the preamplifier pulse shapes and change them into the pulse shapes required for optimum energy spectroscopy. Essentially, its purpose is magnify the amplitude of the preamplifier output pulse and facilitate accurate pulse amplitude measurements with analog-to-digital converters (ADC) and single channel pulse height analyzers. Additionally its main role is to "shape" the pulses to minimize the risk of overlap between successive pulses. The readout electronics then perform a series of an event by an event analysis to sort intensity versus the energy of detected gamma photons yielding a map of electrical pulse height spectrum. Energy resolution is the most important figure of merit in semiconductors which is defined as the ratio of the full-width-at-half-maximum (FWHM) value of that photopeak at a specific energy. Great resolution allows for the distinction between gamma ray photons with a different energy. This is of great importance in applications for homeland security where high energy resolution is expected. [6]

Commercially available semiconductors like that of high purity germanium offer the highest resolution (0.2%) however requires cryogenic cooling due to its low band gap (0.66 eV) that causes dark current. CdZnTe (CZT) offer room temperature application and great resolution (0.5%) however suffer from low bulk resistivity and crystal growth difficulties such as twinning and Te precipitation. TlBr detectors demonstrated high resolution at room temperature as well high bulk resistivity but suffer from polarization effects due to Br- ion mobility which reduce the lifetime and performance of the detectors.[5] Due to the small family of successful gamma radiation detectors, this leaves opportunity for new materials to emerge. Research studies over the past few years have been focusing discovering desirable materials to overcome the limitations discussed above. In the next subsection, we review solution growth methods and the reporting of such methods to growing CsPbBr3 single crystals.

2.2. Low-Cost CsPbBr3 Single Crystal Growth

So many of commercial direct detectors rely on polycrystalline materials which suffer from long reaction times. Complex and expensive melt growth techniques are thus required to grow single crystals of CdTe and CZT that provide desirable high Z semiconductors for gamma detection. The

search for low-cost highly sensitive detectors which operate at room temperature is of great importance to compete with the performance of commercial ones. Due to the small family of semiconductors for gamma detection, perovskite single crystals have been of interest due to better optoelectronic properties than their polycrystalline film counterparts (lower trap density and absence of grain boundaries). Luckily, perovskite single crystals not only provide higher Z components but have demonstrated to be grown by low-cost solution methods. The solution growths were widely used to grow hybrid perovskites as melt growth techniques were not viable due to instability of organic compounds around their melting temperatures. Hybrid perovskites already demonstrated millimeter to centimeter dimension can be grown using different solution-based methods at low temperatures.[7]

Inorganic perovskites do not face this obstacle as they are more stable and first reporting of melt growth of single CsPbX3(X=Cl, Br) crystals using Bridgman technique were achieved as mentioned above. [8,9] However, the work of Stoumpos et al. did not deliver the detection of highly resolved gamma rays due to phase transition after crystallization caused from melt growth. Despite the phase transitions resulting in a high density grown-in defects, subsequent work from the same research group optimized the crystal growth process over multiple growth runs for an improved CsPbBr3 single crystal growth. [10] This ultimately achieved at the time the best spectral resolution (3.8-3.9%) obtained for any halide perovskites. Compared with melt growth, low temperature solution growth can avoid phase transition, multiple purification processes and provide an alternative low-cost method technique to preparing CsPbBr3 single crystals.[11] Additionally, research motivation lies on the indifference of cost to commercial gamma detectors if melt growth methods are used as well.

Perovskite single crystals can be grown from aqueous solutions most famously with a solution temperature lowering (STL) method, an inverse-temperature crystallization (ITC) method and an anit-solvent vapor assisted crystallization (AVC) method. In STL method, millimeter small crystals are synthesized followed by seeded growth for full large size bulk crystals. Depending on the different fixed positions of the seed crystals, a bottom or top seeded solution growth is adopted in which solution temperature is decreased from high temperatures to a saturated state which single crystals begin to form. In ITC method, crystallization is caused by the inverse solubility dependence on temperature in some organic solvents. Raw chemicals are dissolved in organic solvents such as DMSO or DMF at room temperatures followed by incremental increase of temperature to the point of nucleation when the solution come to supersaturation followed by crystal growth. Overall growth in ITC method is much faster (several hours) than the STL method which typically takes days to week to produce high quality single crystals. The AVC method takes the advantage of perovskite's preferred solubility in different solvents. Then, an appropriate anti-solvent is slowly diffused into the solution containing the target precursors. This leads to the nucleation and growth of crystals. [12, 13]

There are few works that demonstrate solution-growth CsPbBr3 single crystals. The AVC method was used by Rakita et al. from a DMSO precursor solution with 1:1 molar ratio of CsBr and

PbBr2.[7] The solutions were titrated by the two anti-solvents MeCN or MeOH at MeCN:DMSO and MeOH:DMSO ratios of 1.1:1 and 0.55:1, respectively, until saturation. Crystal formation occurred at room temperature and growth could be accelerated by heating the antisolvent bath. H_2O was also investigated as an antisolvent and was deemed unfit due to inclination of the orange crystals to blench. Zhang et al. modified the AVC method of CsPbBr3 crystal growth using diluted MeOH solution with DMSO (50% mole ratio of MeOH) as antisolvent to reduce the MeOH vapor pressure which decreased the CsPbBr3 crystal growth rate effectively.[11] This resulted to centimeter sized crystals as opposed to millimeter sized ones in previous reports. Dirin et al. presented the growth using ITC under ambient atmosphere using DMSO which is reported to be the optimal solvent for CsPbBr3 growth.[14] Millimeter size crystals were obtained and were tested for gamma detection. However broad peak using a 241Am gamma source was not observed until the crystal was cooled to 220 K thus leaves room for improvement for room temperature operation. In the remaining sections, we provide the work of Lei et al. in 2020 which was motivated to fill such improvement based on DPP. Lack of such reporting in the context of spectroscopic performance in the work requires a brief overview of the digital based method first.

2.3. Digital Pulse Processing:

For semiconductors, the output signal is a low-amplitude short duration current pulse. Thus, a charge sensitive preamplifier (RC feedback preamplifier) is used to convert this charge pulse into a voltage pulse to be processed by the electronics that follow. This type of preamplifier which is used in this work produces an exponential voltage pulse as the charge decays to the feedback circuit (with decay time τ_F=50 μs). The most important information from the preamplifier is 1) rise time of the preamplifier which represents the charge collection time and 2) the amplitude which represents the energy of the detected radiation. Therefore, the discharging phase represented by the exponential decay is of little value in the energy spectrum and only important in the electronics for discharging purposes. In analog pulse processing systems, the preamp signal from the detector is shaped, filtered, amplified by a shaping amplifier, and then digitized by a peak sensing analog-to-digital converter (ADC). The issue with analog based systems lies in the charge collection stage and the pulse-shaping step. If transit time (fast component of the charge collection) of the detector is comparable to that of the preamplifier decay constant, a loss of output signal occurs known as a ballistic deficit. Additionally, if the transit times are longer than the predetermined shaping amplifier time constant, a ballistic deficit is inevitable. [4]

In digital pulse processing systems (DPP), the detector signal form is digitized immediately and shaped digitally then a pulse height is extracted.[6] The digital processor can be either a field programmable gate array (FPGA) or digital signal processor (DSP). It is noted in this work that FPGA is used which can operate in real time with more flexibility and considers the generated signal on a pulse-by-pulse basis to enhance the spec tropic performance. Digital deconvolution techniques are used in DPP to obtain the impulse response of the detector. The deconvolution

process recovers the detector signal from the convolution of the detector current signal with the impulse response of the preamplifier. Before the deconvolution process begins and after digitization of the preamplifier waveforms, it must be noted that a digitized pole-zero cancellation is implemented to eliminate pulse undershoot. Pole-zero cancellation is already embedded in the most shaping amplifiers in analog pulse processing systems. This is necessary in the case of RC preamplifiers where a long exponential decay cause small amplitude undershoots. The deconvolution of these pulses can be performed using simple digital differentiation as described in [15]. After obtaining the deconvolution signals, it then passed through a Savitzy-Golay (SG) filter which is a low pass filter based on the least-squares polynomial approximation to cancel noise which is restored as well (frame size 9; polynomial order 1). Since the digital processor is FPGA, the coefficients of SG filtering are pre-calculated which afterwards the SG filter is implemented as standard finite infinite response filter (FIR) filter. Filtering the original preamplifier signal before shaping increases signal to noise ratio and reduces the baseline drifts in the shaped signal that is caused due to noise. The implementation of signal filtering functions is not possible through traditional analog signal processing. As count rate increases, the resolution degrades in analog systems whereby digital filter algorithms require less overall processing time which maintains constant resolution over a large range of count rates. Since the detector signal was digitized much earlier in the signal processing chain, this minimizes drift and instability associated with analog signal processing. [6]

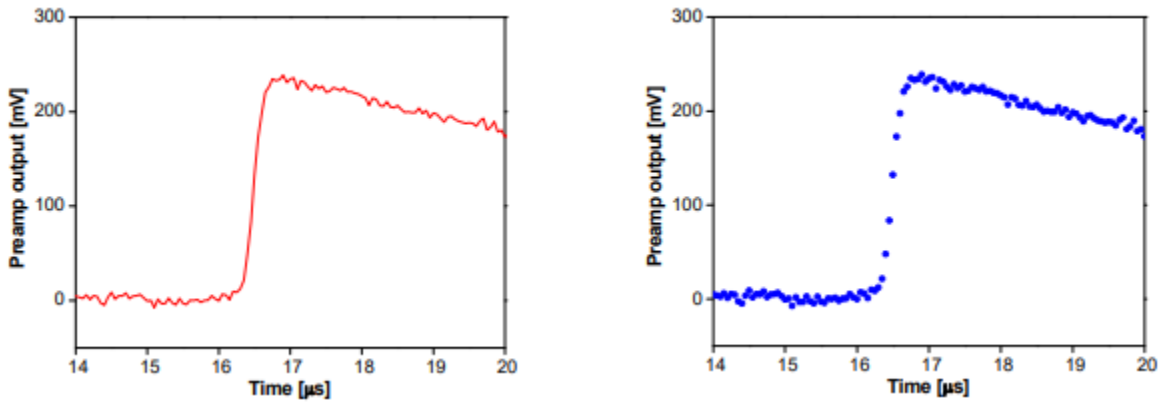

Figure 2. Signal pulse from preamplifier and its digitized form. [16]

Figure 2 shows a simple output pulse of the preamplifier following a detection event and its digitized form. An appropriate digital filter can now be performed for shaping the deconvoluted signal which is required to determine the height of the signal with an optimum signal to noise ratio. The simplest of digital filters is known as the moving average filter. This filter takes the average value for a data length L, such that $V_{avg}[i] = \frac{1}{L}\sum_{j=0}^{L-1} V_{in}[i+j]$ which immediately filters the high frequency noise component, smoothing the original data. However, for shaped pulses that has a long tail and low frequencies that are not attenuated, a more popular type of the digital filter known as trapezoidal filter is used.[16] The principle of this filter is as follows:

For the i^{th} input data point $V_{in}[i]$,

1) Compute the average value for the next L data points,

$$V_{avg1}[i] = \frac{1}{L}\sum_{j=0}^{L-1} V_{in}[i+j]$$

The interval Δt_L is the time interval corresponding to the data length L.

2) Make a separation gap of G data points and compute another average for the data length L,

$$V_{avg2}[i] = \frac{1}{L}\sum_{j=0}^{L-1} V_{in}[L+G+i+j]$$

The interval Δt_G is the time interval corresponding to the data length G.

3) The output signal $V_{out}[i]$ corresponding to the input point $V_{in}[i]$ is computed by,

$$V_{out}[i] = V_{avg2}[i] - V_{avg1}[i]$$

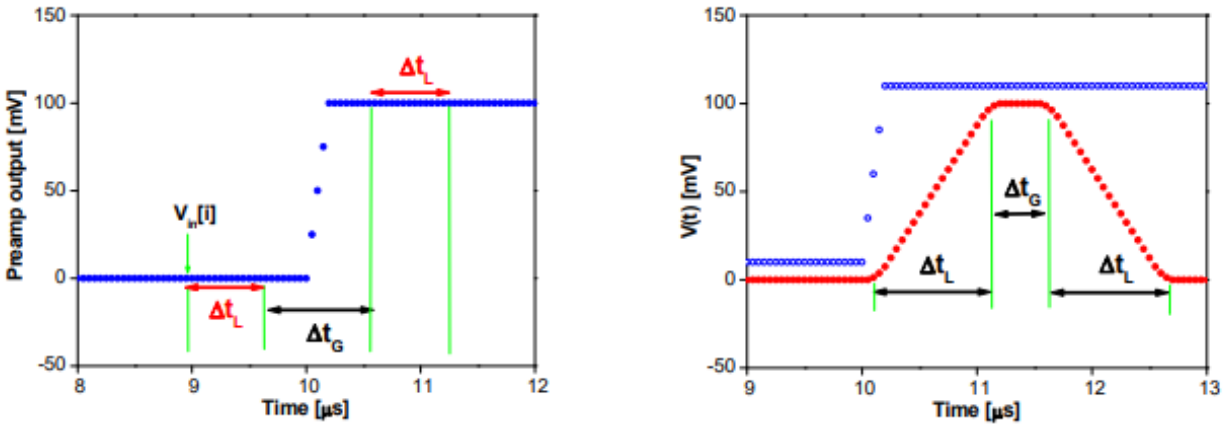

Figure 3. Trapezoidal filter parameters and the filter output. [16]

When this operation is applied to all the input data points, the output pulse shape becomes trapezoidal, as shown in Figure 3. The output pulse has a peaking time equal to Δt_L, a flat top equal to Δt_G, and a symmetric fall time equal to Δt_L. These values can be employed as free parameters to adjust the output pulse shape similar a shaping time used in the semi-Gaussian analog shaping in the analog based electronics. Radioactive decay is a random process, and the radiation pulses follow an interval distribution based on its random nature. The interval distribution can be used to adapt the shaping free parameters mentioned earlier on a pulse-by-pulse basis.[6] Therefore, before implementation of the trapezoidal shaping filter, the

exponential signal is synthesized to define a linear time invariant recursive system to an input signal such that,

$$Y(z) = G(z) + az^{-1}Y(Z) \quad (4)$$

where a is the exponential base and $G(Z)$ is the deconvoluted signal, as an input to generate the exponential pulse. For digital filtering, it is preferred to use linear z transform. Its definition and properties are outside the scope of this work. The generated exponential signal has a rise time constant which represents the charge collection time of the original signal and a decay time constant which represents a value much smaller than the preamplifiers decay time after going through the pre-shaping filters mentioned above. These values are incorporated in the trapezoidal shaping algorithm with Δt_L set to be adaptive according to the time interval of separation between preamplifier pulses while Δt_G is adaptive according to the charge collection time of the detector. Literary works have long praised this popular filter for semiconductors since signals consist of variable rise times which depends upon charge collection time. Therefore, the optimum filter for semiconductors is a trapezoid filter with a flattop larger than the charge collection time to compensate the ballistic deficit. For illustration, Figure 4 shows a normalized amplitude MATLAB simulation of the algorithms including digital pole-zero cancellation, digital pulse deconvolution, SG filter, exponential signal generator, and trapezoid shaping for a RC preamplifier. [6]

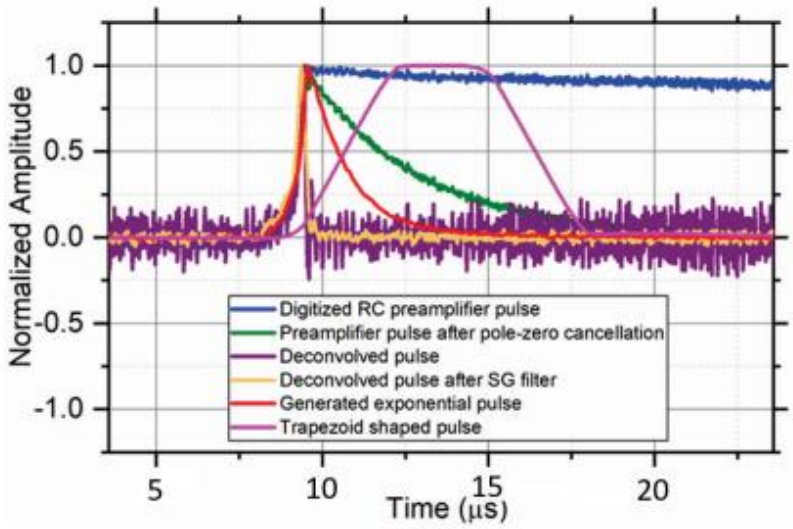

Figure 4. Implementation of digital pole-zero cancellation, digital pulse deconvolution, SG filter, exponential signal generator, and trapezoid shaping for a RC preamplifier.[6]

3 SUMMARY OF WORK

Improvement based on such detector's gamma ray spectroscopic performance based on conventional analog-based nuclear instruments compared to digital-based methods is the main topic of this report. In this work, Lei et al. has grown $CsPbBr_3$ crystals based on the ITC method. The crystals were synthesized by dissolving 3.523 g PbBr2 and 1.021 g CsBr into 5.5-mL Dimethyl

sulfoxide (DMSO) at 100 ◦C for one growth. The solution was then filtered with a 0.2 μm polytetrafluoroethylene (PTFE) filter, and heated at 115 ◦C for 48 to 72 h to grow large crystals. The devices were finished by evaporating a 50-nm Au electrode on one side of the crystal and applying the Ga electrode on the other side. I-V curve showed a Schottky function and the setup was made under reverse bias. Design of the asymmetric electrodes and device structure has been established in achieving a low dark current. For a p-type $CsPbBr_3$, a low work function (WF) is necessary to form a Schottky-barrier based on an asymmetric electrode configuration that can dramatically reduce the dark current by at least three orders of magnitude. [10]

In an effort analyze the energy spectral performance of gamma ray detectors, Lei et al. demonstrated a comparative study of energy spectra of parallel plate Au/CspbBr3/Ga detectors using conventional analog-based nuclear instruments to one using a digital-based method known as digital pulse processing (DPP). Solution growth of CsPbBr3 crystals were used for three planar detectors, detector I (2.53 × 7.08 × 8.29 mm3), detector II (2.3 × 5.54 × 6.21 mm3), and detector III (3 × 7.35 × 7.35 mm3). Au and Ga electrode area of 4.5 × 4.5 mm2 were centered on each detector's respective surface hence, an effective detection volume of 2.53 × 4.5 × 4.5 mm3 for detector I and so forth for the rest of the detectors. A CZT detector, with roughly the same effective detection volume, was also fabricated with the same electrode structure for comparison. This was chosen since CZT and CsPbBr3 detectors resemble each other in their unbalanced electron and hole transport; hole μτ product is lower than that of the electron for CZT and the opposite is true for $CsPbBr_3$ based on previous work, see Table 1. [10, 17] This was anticipated in this work as well and its effect on the gamma ray energy spectra is evaluated.

Table 1. CsPbBr3 single crystal electron and hole transport μτ product based on previous work. [10, 17]

$(\mu\tau)_e$	$(\mu\tau)_h$	Reference
$8.77 \times 10^{-4} \frac{\mathrm{cm}^2}{V}$	$1.34 \times 10^{-3} \frac{\mathrm{cm}^2}{V}$	10
$4.5 \times 10^{-4} \frac{\mathrm{cm}^2}{V}$	$9.5 \times 10^{-4} \frac{\mathrm{cm}^2}{V}$	17

Analog-based nuclear instruments acquires energy spectra from a preamplifier connected to a shaping amplifier connected to an analog-to-digital converters (ADC) embedded multi-channel analyzer (MCA). The digitized method applies digital filters to digitize raw waveform signals at post preamplifier stage then to a digital deconvolution stage to optimize signal to noise ratio. This does not only eliminate the need for shaping amplifiers and pulse height sorting by MCA, it can be effective to deal with the convoluted signals that are caused by the pile up of pulses from high count rates associated with the gamma intense sources. Since CsPbBr3 current transit times were reported to be several microseconds under a range of electric field ~400–800 V/cm from previous studies, it is understood that energy distortion, due to ballistic deficit, will appear if preamplifiers as well as shaping amplifiers time constants are not suitably chosen. Therefore,

DPP shows more flexibility if transit times or full charge collection times are longer than the shaping amplifier's time constant. Transit times are obviously dependent on material property but at a given thickness, its impact must be understood. Figure 5 shows the schematic block diagram of the detection systems used in this work. A Monte Carlo simulation was performed in Geant4 to simulate source-detector configuration with detector I and a Cs-137 gamma source to highlight the importance of detector thickness and its effect on peak-to-Compton ratio, an important parameter for gamma detection. Detector thickness was simulated for 25.3 mm, 2.53 mm, and 0.253 mm and the energy spectra showed that as thickness decreased, high Compton continuum is observed which leads to a low peak-to-Compton ratio. It a desired figure of merit for gamma ray detection to have a high peak-to-Compton ratio.[3]

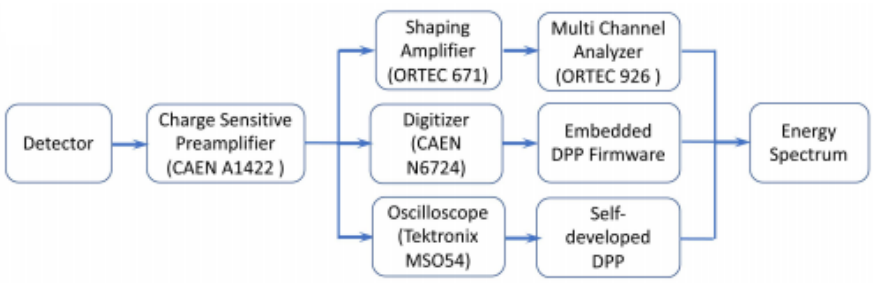

Figure 5. Schematic block diagram for three experimental setups; analog, digitizer, and oscilloscope in waveform mode. [3]

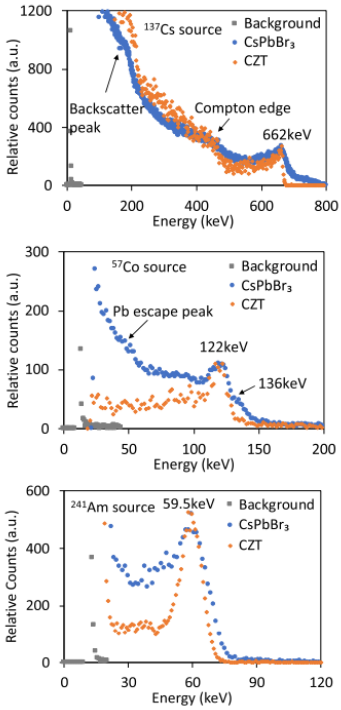

Figure 6. Comparison of Cspbbr3 detector I and commercial CZT detector gamma spectra using analog instrumentation.[3]

Using the analog spectroscopy system, gamma ray spectra of CsPbBr3 based on detector I was acquired with FWHM of 5.5% at 662 keV for 137Cs, 13.1% at 122 keV for 57Co, and 28.3% at 59.5 keV for 241Am with energy linearity R2 nearly equal to unity. CZT detector resembled similar results, see Figure 6, which implied that the limiting factors of energy resolution on CZT are the same in CsPbBr3 spectra, i.e., different electron/hole transport property and size effect. To investigate the transport property further, the research group used the gamma energy sources at two positions (above and below) relative to the detector to observe the degradation of energy resolution that depended on penetration depth of the gamma energy photons. It was evident that lower energy sources, given its limited penetration length i.e., <10% transmission over the first 1-mm thickness for 241Am, yielded better energy resolutions for mainly hole transport where the sources were placed over the Ga electrode. However, 137Cs gamma ray photons did not have this effect since its charge carriers were generated uniformly through the detector due to its greater penetration depth. Figure 7 shows the gamma ray energy spectra based on the investigation of the electron/hole transport property using source-to-detector configurations. This unbalanced electron and hole transport is manifested in lower energy tailing in CZT spectra and the asymmetric Gaussian shape for full energy peaks in CsPbBr3 spectra, see Figure 6. The longer tail in the high energy end of the photopeak in CsPbBr3 spectra can be associated with noise and higher statistical variance in charge carrier generation due to the higher bandgap of CsPbBr3. [3]

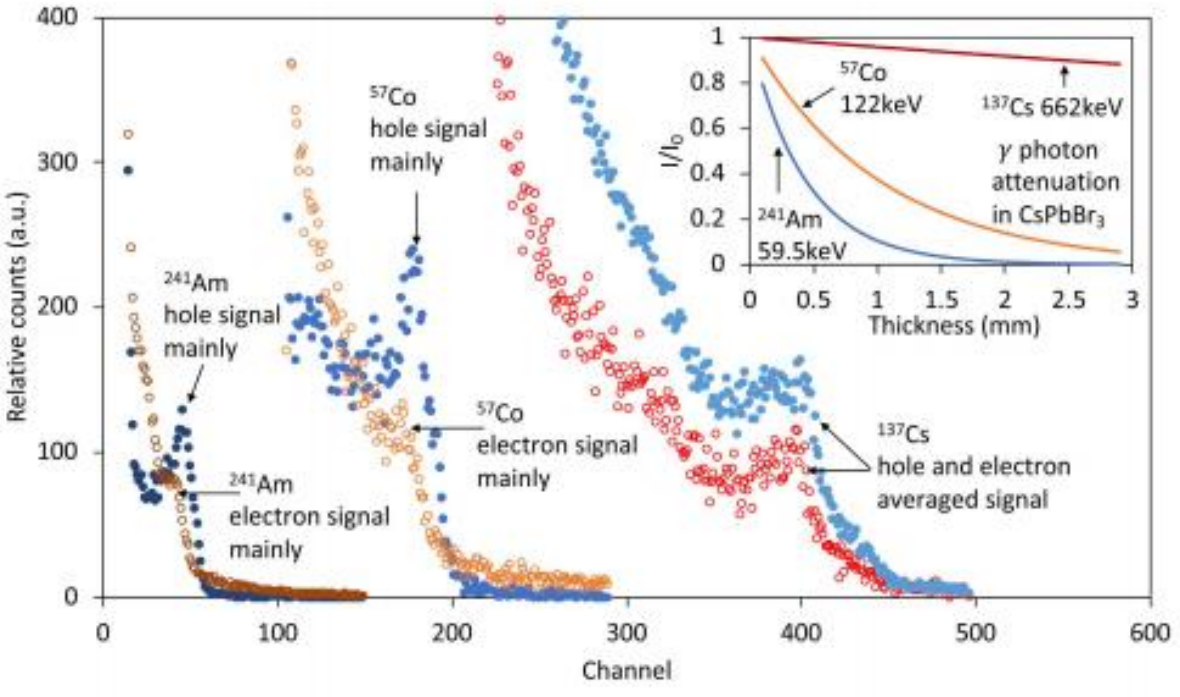

Figure 7. Analysis of electron and hole transport properties acquired by $CsPbBr_3$ detector I.[3]

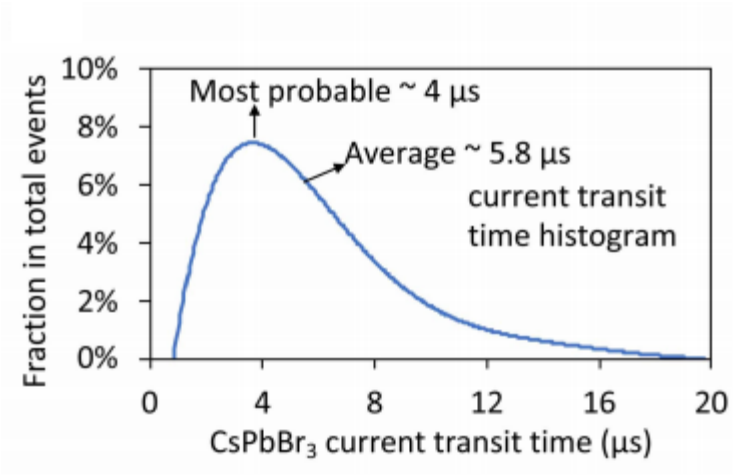

Figure 8. Histogram of the current transit time of $CsPbBr_3$ detector I under 500 V with 137Cs γ source.[3]

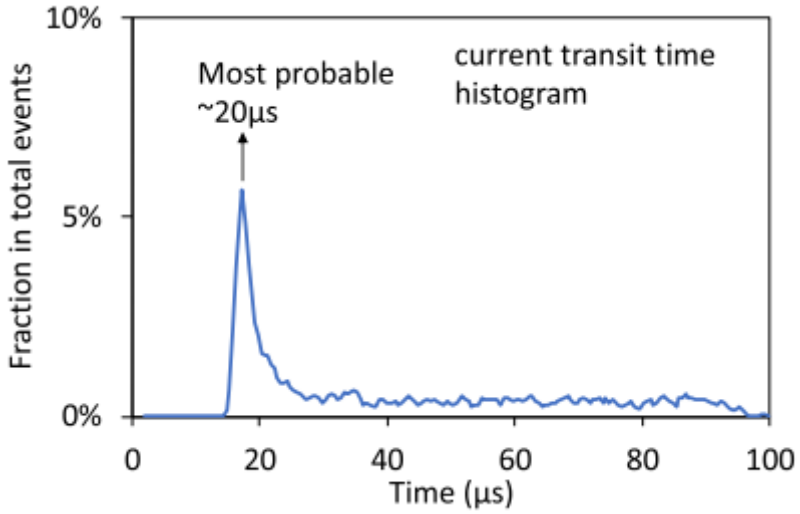

Figure 9. Histogram of current transit time of $CsPbBr_3$ detector II at 50 V with 137Cs source.[3]

An average transit time of 5.8 µs was evaluated for detector I at 500 V with 137Cs gamma source and at 50 V with the same source, detector II most probable transit time was evaluated at 20 µs, see Figures 8 and 9, respectively. Detector III was evaluated at 20 µs for a 600 V bias with 137Cs gamma source and its histogram is not provided in the work. Current transit time can be reduced by applying a higher bias voltage but this would increase noise and worsen the spectral performance. Therefore it the aim of the work to understand the spectral performance given these transit times according to the bias applied.

The charge collection efficiency of CsPbBr3 detector I at 800 V with a 137Cs gamma source was estimated by taking the ratio of experimentally measured collected charge to the theoretically generated charge. This ratio essentially represents the fraction of charges which reaches the electrodes. Theoretical charge can be calculated as $Q_o = 662\ keV * \frac{e}{W}$, where "$e$" is the elementary charge and W is the average electron–hole pair creation energy (W-value) evaluated through an empirical equation $\mathrm{W} = 2.73 * \mathrm{E_g} + 0.55, (\mathrm{E_g} = 2.23\ \mathrm{eV\ for\ CsPbBr_3})$. Experimentally measured charge for CsPbBr3 was calculated using a calibrated fitted relationship between charge and channel number obtained by CZT saturated photo peak channels to varying gamma ray energies. Knowing the channel of 662 keV gamma peak in the CsPbBr3 detector I, the collected charge was calculated. CCE was estimated to be 92.3%. The incomplete charge collection may be attributed the inefficient electron collection.[3] This also highlights the importance of evaluating the W value for a more accurate estimation of CCE. In the limit of no de-trapping and a uniform electric field, the voltage dependence of the CCE can be described by the single carrier Hecht equation,

$$CCE = \frac{\mu\tau V}{d*x}[1 - \exp(-\frac{d*x}{\mu\tau V})] \quad (5)$$

where d is the detector thickness, x is the estimated average distance that charge carrier drifts to reach the collecting electrodes, V is the applied bias voltage, and μ, τ are the mobility and lifetime of either electrons or holes. Therefore, Hecht equation fitting can be used to estimate μτ product. In order to use this equation, a near surface charge is necessary such that only one carrier is considered when charges are collected under bias and consequently x is taken as d. In this work, a near surface charge was not a viable option due to thickness of Ga electrode (1-2 mm thick) which prevented small penetration sources like alpha particles or X-rays to be used. Instead, a 137Cs gamma source was used due to the greater penetration length and the assumption of charge carrier generation uniformly inside the detector volume in which case x is taken as $\frac{d}{2}$. CCE vs Voltage plot of CsPbBr3 detector I was obtained for fitting according to the relationship of peak channel number versus applied voltage. The estimated average μτ is $4.0 \times 10^{-4}\ \frac{\mathrm{cm}^2}{V}$ accordingly which is similar to previous reporting, see Table 1. The average transit time value given in Figure 8 was used to estimate the average electron-hole mobility by the equation $t_r = \frac{d^2}{\mu V}$ to be $22\ \frac{\mathrm{cm}^2}{V\ s}$.

DPP algorithms offered a versatile way to circumvent this issue by dealing with digitized waveforms signals at post preamplifier, see Figure 10. A deconvolution technique, using mathematical filters and shaping parameters for each incoming signal, essentially reconstructs the original detector's signal by canceling the convolution of the detector signals with the impulse response of the preamplifier. Then the energy spectrum is reconstructed by calculating the deconvoluted signal amplitudes directly from the difference between the signal peak and the baseline value. [3]

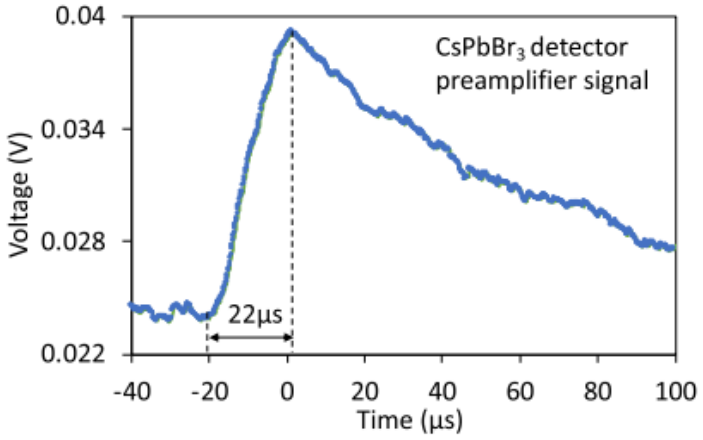

Figure 10. Preamplifier waveform signal of CsPbBr3 detector II at 50 V with 137Cs source.[3]

DPP algorithm's capability was first validated for CZT detectors, established smaller transit times compared with preamplifiers decay constant (50 µs), for gamma ray energy spectrum compared to its counterpart spectrum using the analog method. After observing validation through the level of agreement between two types of spectra and the DPP algorithms effect on reducing distortions, it was applied to the reconstruction of distortion-free energy spectra of CsPbBr3 detectors with different transit times, see Figure 11. For detector II and III where the transit times on average are 20 µs, the reconstruction of the spectra shows observable photo-peaks that otherwise would have been lost as seen by the analog spectroscopy system. Detectors I showed little impact from ballistic deficit due to the average transit time of 5.8 µs which is one order of magnitude lower than the preamplifier's decay constant but nonetheless proved that DPP produces a more tolerant and versatile energy spectrum. [3]

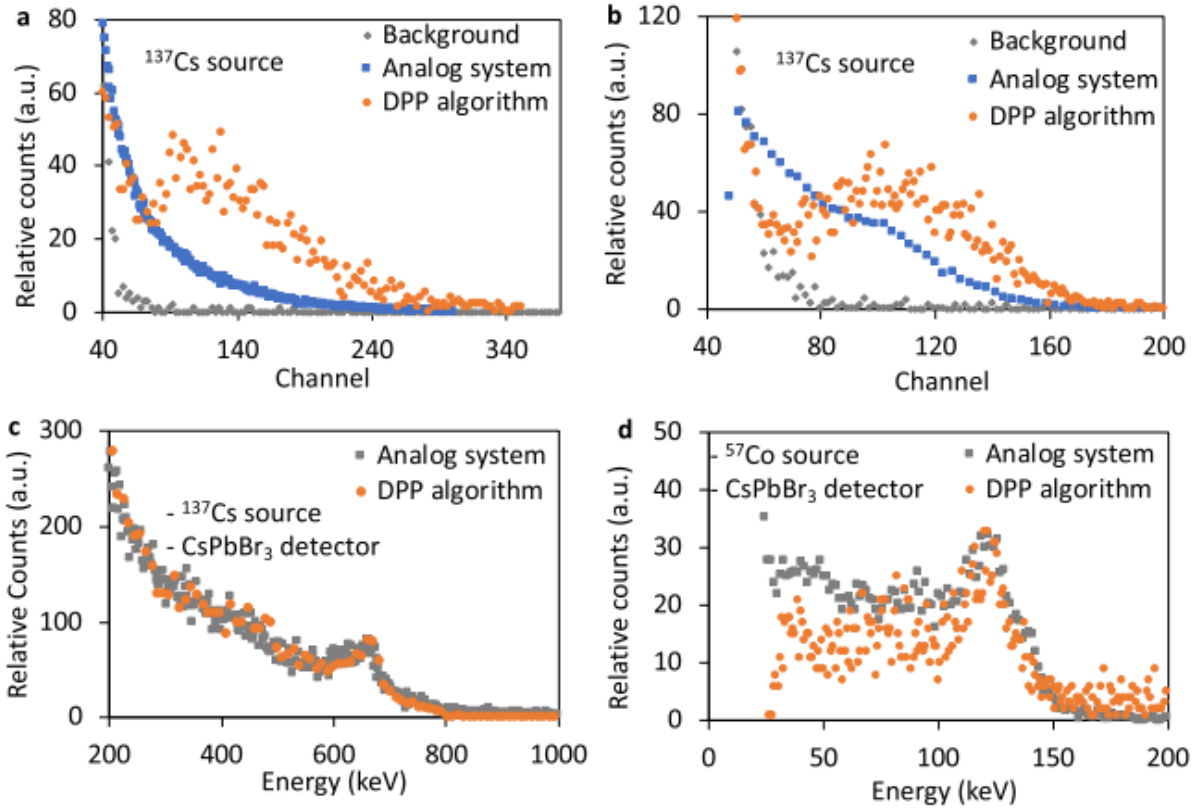

Figure 11: Gamma -ray energy spectra of CsPbBr3 detectors with different current transit times acquired using the analog spectroscopy system and reconstructed by the DPP algorithm. (a) Comparison of 137Cs gamma -ray energy spectrum of CsPbBr3 detector II (2.3 × 5.54 × 6.21 mm3) with current transit time of ~20 µs at 50 V (see Fig. 9). (b) Comparison of 137Cs gamma -ray energy spectrum of CsPbBr3 detector III (3 × 7.35 × 7.35 mm3) with current transit time of ~20 µs at 600 V. (c) Comparison of 137Cs gamma -ray energy spectrum of CsPbBr3 detector I (2.53 × 7.08 × 8.29 mm3) with current transit time of ~5.8 µs at 500 V [see Fig. 8]. (d) Comparison of 57Co gamma -ray energy spectrum of CsPbBr3 detector I (2.53 × 7.08 × 8.29 mm3) with current transit time of ~5.8 µs at 500 V [see Fig. 8].[3]

CRITIQUE

This work has achieved its set goal in terms of analyzing the spectroscopic performance of $CsPbBr_3$ crystals. Not until the reporting of this work was it available for researchers the versatile way DPP can produce the similar or better resolution for detectors with different transit times of $CsPbBr_3$ single crystals. Material preparation in this work has proved that low defects of single crystals can be achieved without degradation of resolution as in previous work. This provides researchers a great methodology for single crystal growth since resolution of gamma photo peaks

were not achievable without melt growth methods. Furthermore, since passivation was not explicitly stated in the preparation of crystal growth, researchers might take notice of the superiority of preparing the low defect crystals. Previous studies have highlighted the importance of single crystal defects arising from solution growth and the role of passivation to counter this factor. Little mention was reported on the conditions of environmental exposure when preparing the crystals. For μτ product calculation, the research group used the single carrier Hecht equation although limitation of its use was noticed. While hole transport property could not be accurately estimated due to the thickness Ga electrode, electron transport properties could be accurately estimated using a bias dependent alpha particle spectra where a source could be placed under the Au electrode. Nonetheless, a thermal evaporation method of attaching the Ga electrode in the nm range is best as was reported in previous studies. The investigation of the unbalance electron and hole transport was clearly explained. The research group provided not only the average transit time but a probable transit time for the best spectral performance by detector I which from the histogram which can be used for statistical analysis. Validation of the DPP algorithm using CZT commercial detector gave confidence to DPP deconvolution technique as an established method to circumvent the ballistic deficit issue. Little mention was made to the reason comparable average times were achieved for detectors I and III which were under more than an order of magnitude of difference in voltage bias. It is not explicitly mentioned whether the insignificant differences of the detector thicknesses played a role.

CONCLUSION

In this critique review, we briefly introduce the role of perovskites for wide range radiation detection. We list the major figure of merits for gamma detection for semiconductors and prospect of halide perovskites especially inorganic ones to fulfill the requirement in commercializing the new generation of semiconductors. We briefly mention the few works that have conducted for solution growth of $CsPbBr_3$ single crystals and the room for improvement for further studies in this exciting material. Then we provided the theoretical background of DPP and the shaping filters in contrast to the analog based methods. After that, we provide a summary of Lei et al. reported work which was motivated to provide consistency on gamma ray spectroscopic performance using DPP compared to analog based nuclear instruments. Gamma ray spectra is achieved from the CsPbBr3 detector using 137Cs, 57Co, and 241Am sources with 5.5% FWHM at 662 keV, 13.1% FWHM at 122 keV, and 28.3% FWHM at 59.5 keV, respectively. A Hecht equation fit to the CCE versus detector bias plot from 137Cs energy spectra was used to estimate the averaged electron-hole μτ product and was evaluated to be $4.0 \times 10^{-4} \frac{\mathrm{cm}^2}{V}$. It is noted that the single carrier Hecht equation was used knowing that a near surface charge generation could not be acquired due to the thickness of the Ga electrode. Averaged electron-hole mobility was estimated to be $22 \frac{\mathrm{cm}^2}{V\,s}$. DPP algorithm's capability was validated on established CZT detector first. It was then applied to reconstruct the energy spectra of $CsPbBr_3$ detectors with different transit times and applied bias.

Since detector I had a transit time (5.8 μs) that was almost an order of magnitude less than the preamplifier constant (50 μs), similar energy spectra was observed when compared to using analog systems thus less distortions to deal with due to ballistic deficit. However, major reconstruction was observed for detectors II and III when the peaks were noticed even though it was broadened. This work provides proof that DPP is a more tolerant and versatile way of producing energy spectrum than those produced by an analog system.

REFERNCES

[1] Kakavelakis, George, et al. "Metal Halide Perovskites for High-Energy Radiation Detection." *Advanced Science* 7.22 (2020): 2002098.

[2] McCall, Kyle Matthew. *Synthesis, Crystal Growth, and Optoelectronic Characterization of Inorganic Halide Perovskites as Semiconductors for Hard Radiation Detection*. Diss. Northwestern University, 2019.

[3] Pan, Lei, et al. "Performance of Perovskite CsPbBr 3 Single Crystal Detector for Gamma-Ray Detection." *IEEE Transactions on Nuclear Science* 67.2 (2020): 443-449.

[4] Knoll, Glenn F. *Radiation detection and measurement*. John Wiley & Sons, 2010.

[5] Zhang, Zheng, and Ge Yang. "Recent advancements in using perovskite single crystals for gamma-ray detection." *Journal of Materials Science: Materials in Electronics* (2020): 1-13.

[6] Saxena, Shefali. "Adaptive Digital Pulse Processing for Real-time High-throughput High-resolution Gamma-ray Spectrometry." (2019).

[7] Rakita, Yevgeny, et al. "Low-temperature solution-grown CsPbBr3 single crystals and their characterization." *Crystal Growth & Design* 16.10 (2016): 5717-5725.

[8] Stoumpos, Constantinos C., et al. "Crystal growth of the perovskite semiconductor CsPbBr3: a new material for high-energy radiation detection." *Crystal growth & design* 13.7 (2013): 2722-2727.

[9] Kobayashi, M., et al. "Scintillation characteristics of CsPbCl3 single crystals." *Nuclear Instruments and Methods in Physics Research Section A: Accelerators, Spectrometers, Detectors and Associated Equipment* 592.3 (2008): 369-373.

[10] He, Yihui, et al. "High spectral resolution of gamma-rays at room temperature by perovskite CsPbBr 3 single crystals." *Nature communications* 9.1 (2018): 1-8.

[11] Zhang, Hongjian, et al. "Centimeter-sized inorganic lead halide perovskite CsPbBr3 crystals grown by an improved solution method." *Crystal Growth & Design* 17.12 (2017): 6426-6431.

[12] Li, Shuigen, et al. "Metal halide perovskite single crystals: from growth process to application." *Crystals* 8.5 (2018): 220.

[13] Ding, Jie, and Qingfeng Yan. "Progress in organic-inorganic hybrid halide perovskite single crystal: growth techniques and applications." *Science China Materials* 60.11 (2017): 1063-1078.

[14] Dirin, Dmitry N., et al. "Solution-grown CsPbBr3 perovskite single crystals for photon detection." *Chemistry of Materials* 28.23 (2016): 8470-8474.

[15] Jordanov, Valentin T. "Unfolding-synthesis technique for digital pulse processing. Part 1: Unfolding." *Nuclear Instruments and Methods in Physics Research Section A: Accelerators, Spectrometers, Detectors and Associated Equipment* 805 (2016): 63-71.

[16] Byun, Soo Hyun. "Med Phys 4RA3, 4RB3 & 6R03 ." 2018. Chapter 6 Pulse Processing. <https://www.science.mcmaster.ca/radgrad/images/6R06CourseResources/4RA34RB3_Lecture_Note_6_Pulse-Processing.pdf>.

[17] He, Yihui, et al. "Perovskite CsPbBr3 single crystal detector for alpha-particle spectroscopy." *Nuclear Instruments and Methods in Physics Research Section A: Accelerators, Spectrometers, Detectors and Associated Equipment* 922 (2019): 217-221.